Reprinted from Applied Optics, Vol. 25, Page 4374, December 1, 1986

Airborne measurements of the optical stratification of aerosols in turbid atmospheres

Teruyuki Nakajima, Masayuki Tanaka, Tadahiro Hayasaka, Yukiharu Miyake, Yuji Nakanishi, and Kazutoshi Sasamoto

A spectral scanning radiometer and corresponding algorithm of analysis were developed to evaluate optical stratification of aerosols from airborne measurements. Several flights were carried out to measure direct and circumsolar radiations simultaneously by a Swerlingen Merlin IV and a Cessna 206 aircraft. Results of the data analysis showed that our scheme can evaluate the optical depth of aerosols at any flight level from the ground to 400 mb, the highest flight level, with relative error of <10%. Vertical distribution and latitude–height cross sections of the optical thickness of aerosols and volume spectra of stratospheric aerosols were investigated.

I. Introduction

Climatic perturbation due to stratospheric aerosols of volcanic origin has been a lively topic of discussion after the big eruptions of Mt. St. Helens and El Chichon. Changes in the radiation budget of the earth–atmosphere system with an increase in the optical thickness of stratospheric aerosols may be the most direct and obvious result in complex mechanisms of the perturbation.[1–4] Optical stratifications of the enhanced stratospheric aerosol layer due to El Chichon eruption were successfully measured by airborne sunphotometers.[5–8] An advantage of sunphotometry is the possibility of retrieving the size distribution and optical thickness of aerosols, which are required to evaluate the transfer of solar radiation in an aerosol laden atmosphere.[9,10]

Although the airborne sunphotometer is a powerful tool for monitoring global scale turbidity, the most serious difficulty in achieving the accuracy required for determination of the optical thickness of aerosols is to maintain the calibration constant of the instrument.[11–13] An alternate but closely related approach to this problem is to use circumsolar radiation (or aureole) measurements. Monitoring the atmospheric turbidity[13–17] and retrieving the aerosol size distribution from the circumsolar radiation or from combined data of direct solar and circumsolar radiations have been investigated by many workers.[18–23] An advantage of the use of the aureole intensity is that the aureole intensity is approximately proportional to the aerosol optical thickness, although easy use of this method has been obstructed by difficulty in removing multiply scattered radiation and enlargement of the optical system of the radiometer.

In this paper we describe a compact seven-channel aureolemeter newly developed for airborne measurement and an algorithm to retrieve optical properties of aerosols from obtained data. Pioneers of such works are Twitty *et al.*[24] They[24,25] successfully retrieved the size distribution of aerosols at several flight levels from the aureole intensity measured by a single-channel scanning photometer. However, they did not use the absolute scale of the aureole intensity but used the integrating nephelometer data to interpret the backscatter profile obtained by a simultaneous lidar measurement. We rather adopt a self-closed algorithm to determine the optical thickness, volume spectrum, and phase function of aerosols simultaneously from the data of the aureolemeter alone. Realization of the aureolemeter is discussed in Sec. II, and examples of analysis of the data are given in Sec. III, paying attention to retrieval of optical thickness and volume spectrum of aerosols in the upper troposphere and stratosphere.

II. Instrument Design and Algorithm of Analysis

An aureolemeter was compactly assembled within a spherical aluminum container 260 mm in diameter

Teruyuki Nakajima, M. Tanaka, and T. Hayasaka are with Tohoku University, Upper Atmosphere Research Laboratory, Sendai 980, Japan; the other authors are with Eko Instruments Company, Ltd., Tokyo 151, Japan.

Received 14 March 1986.
0003-6935/86/234374-08$02.00/0.

Table I. Specifications of the Aureolemeter

Interference filters: Koshin Kogaku Co., BWWB series with wavelengths (half width) of 332(5),368(9),500(2),675(3),777(2),862(5),937(5) (nm) blocking in both wings: <0.01% in transmittance for all filters
Detector: Hamamatsu Photonics Co., PIN silicon photocell, S1722-02Q Peak wavelength of 900 nm, NEP 6×10^{-14} (W/√Hz)
Optical alignment: Sunphotometer type
Sun-shade hood: 145 mm
Solid view angle: 0.001524
Electrical dynamic range: 10^5
Mount: Altazimuth with 2 axis-motor driving
Mechanical precision of sun-following: 0.25° rmsd

designed to set on a light aircraft. Specifications for the aureolemeter are shown in Table I. Solar radiation through an interference filter on a rotating turret is detected by a ultrafast response PIN silicon photocell. A linear I/V converter was designed to have a dynamic range of 10^5 with five gain stages to detect both the direct and diffuse radiations. The position of the sun is monitored by a 2-D silicon photodiode (Hamamatsu Photonics Co., Silicon Position Sensitive detector S-1200).

The aureolemeter is controlled by a microcomputer (SORD Co. model M/23) and a controller which consists of an A–D converter, data sequencer, and angle controller. The driving system of the aureolemeter has two modes: for the external mode, the host computer can control the altazimuth mount at any direction, while for the automatic mode the aureolemeter automatically follows the sun by zenith/azimuth dc servo motors. Output data, such as seven-channel light signals, detector temperature, zenith, azimuthal angles (θ,φ), and the position of the sun (x,y), are temporally stored in a 16-kbyte RAM during 3 s of scanning solar aureole and are transferred to the host computer through a parallel interface. Three scannings with different I/V converter gains are necessary to cover the variation of the spectral solar aureole intensities at scattering angles of <40°.

We required the flatness of the field of view of the aureolemeter by adopting an optical alignment with no lens as in a Voltz-type sunphotometer, because the direct solar signals fluctuated as the solar image wandered the field of view with rolling and pitching of the aircraft for the case of a prototype of the aureolemeter with an object lens. Figure 1 shows a response function of the field of view defined as a normalized output signal when a plane–parallel beam enters the system. The value of the response function was measured in a laboratory using a filament-type halogen lamp of 300 W located at a distance of 2054 mm from the surface of the detector to attain the view angle of the filament of <0.5°. Four measurements were carried out on two successive days. Observed values of the response function (circles in Fig. 1) were in fairly good accordance with the theoretical profile (lower solid line in Fig. 1) at incident angles of <1.80°. Since the optical

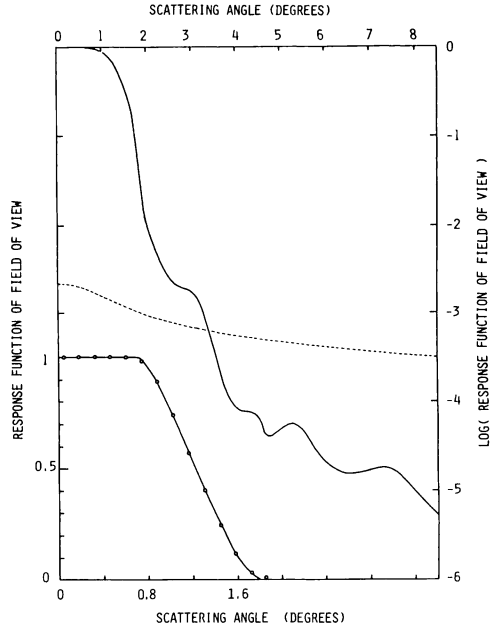

Fig. 1. Response function of the field of view: lower solid line and circles, theoretical and experimental values, respectively, with reference to the lower and left scales; upper solid line, experimental values with reference to the upper and right scales; dashed line, simulated signals calculated by Eq. (1).

alignment of our aureolemeter consists simply of the detector and field stop of which radius r_2 is larger than that of the detector r_1, the theoretical profile of the response function can be calculated by assuming two characteristic angles, i.e., the mean suspending half-angle of the field stop $\theta_1 \simeq r_2/l$ and the maximum incident angle for detection $\theta_2 \simeq (r_1 + r_2)/l$, where l is the spacing between the field stop and detector. Best fit values of θ_1 and θ_2 are 1.26 and 1.81°, respectively, in Fig. 1. The theoretical value of the response function is unity for incident angles of $<\theta_3 = 2\theta_1 - \theta_2$, while the maximum observed deviation from unity was 0.014 at the incident angles of $<\theta_3 = 0.71°$ for all the spectral channels. Since the standard deviation of the mechanical precision of the solar tracking system is ~0.25° for a pitching/rolling rate of ~10°/2 Hz, the width of the flat region of the field of view is sufficient to measure the direct solar radiation with a relative error of <1.4%.

For an ideal sunphotometer with no stray light, no response is expected at incident angles larger than θ_2, while the observed response function was as large as 10^{-3} at the incident angle of 3° as shown by the upper solid line in Fig. 1. Since the sun-shading hood could not be longer than 145 mm for aerodynamic reasons, we could not remove stray light perfectly. The dashed line in Fig. 1 shows a simulated signal calculated by the single-scattering approximation in the solar almucantar as

$$E(\theta) = m\omega_0\tau P(\theta)\exp(-m\tau)F_0 d\Omega, \quad (1)$$

where $F_0,m,\omega_0,\tau,P(\theta),d\Omega$ are the direct solar irradiance at the top of the atmosphere, optical air mass, single-scattering albedo, optical thickness, phase function at

the scattering angle of θ, and a solid view angle of the radiometer, respectively. A Junge-type size distribution of aerosols of optical thickness $\tau = 0.1$ and an optical air mass $m = 2$ are assumed in the simulation. For the solid view angle, we obtained the value of $d\Omega = 1.524 \times 10^{-3} \pm 0.012 \times 10^{-3}$ by integrating the response function in Fig. 1. By this simulation it is seen that the minimum observable scattering angle without serious contamination of the stray light is ~5° or larger for the case shown. In the analysis of the real data, we discarded contaminated data points comparing the data to the response function in Fig. 1.

Since the aureolemeter observes both the direct and diffuse solar radiations, a normalized intensity can be calculated with the measured solid view angle as

$$R(\theta) = E(\theta)/mFd\Omega, \tag{2}$$

where

$$F = \exp(-m\tau)F_0. \tag{3}$$

Since the normalized intensity $R(\theta)$ is approximately the differential scattering coefficient, $\beta(\theta) = \omega_0 \tau P(\theta)$, as shown from Eqs. (1) and (2), the columnar size distribution of aerosols can be obtained by an inversion technique after removing the effect of multiple scattering due to aerosols and molecules.[22] Although several useful schemes have been developed for calculation of the aureole intensity, these schemes are applicable to the case with a known optical thickness of aerosols. For aircraft measurements, however, it is very difficult to determine the optical thickness from observation of the direct solar radiation due to errors involved in the calibration constants of the radiometer and in the observed intensities which are affected seriously by temperature control under severe flight conditions and the flatness of the field of view. We, therefore, adopt an iteration scheme to determine the optical thickness and intensity of multiply scattered radiation simultaneously from the normalized intensity $R(\theta)$ alone. The normalized intensity is hardly affected by the errors mentioned above.

Basic formulations for the iteration are the same as Nakajima *et al.*[22] but without assuming the optical thickness of aerosols *a priori*. The outline of our scheme is as follows: (1) define initial values of the differential scattering coefficient and the optical thickness of aerosols by measured values of the normalized intensity $R^0(\theta)$ and the optical thickness τ_a^0 for each wavelength as

$$\beta_a^1(\theta) = R^0(\theta) \quad \text{and} \quad \tau_a^1 = \tau_a^0; \tag{4}$$

(2) calculate the intensity $R^n(\theta)$ in the aureole region by a radiative transfer code including the polarization effect,[22,26,27] (3) correct the assumed differential scattering coefficient $\beta_a^{n+1}(\theta)$, comparing the observed normalized intensity with the theoretical one as

$$\beta_a^{n+1}(\theta) = \gamma^n(\theta)\beta_a^n(\theta), \tag{5}$$

where the ratio $\gamma^n(\theta)$ is defined by

$$\gamma^n(\theta) = R^o(\theta)/R^n(\theta); \tag{6}$$

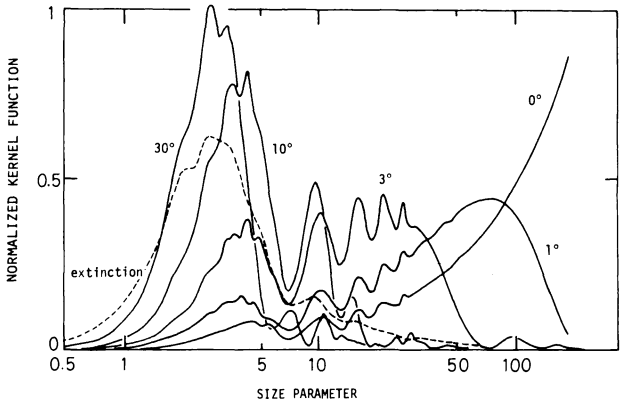

Fig. 2. Kernel functions vs the size parameter kr for the differential scattering cross section at various scattering angles (solid lines) and for the total extinction cross section (dashed line).

(4) retrieve the columnar volume spectrum of aerosols $v(\ln r) = dV/d\ln r$ at particle radius r from the integral equation

$$\beta_a(\theta) = \int K(\theta,x)v(x)dx, \qquad x = \ln r, \tag{7}$$

where the kernel function $K(\theta,x)$ is calculated from Mie's amplitude function $S(\theta,kr)$ as

$$K(\theta,x) = \frac{3}{4r}\frac{|S(\theta,kr)|^2}{\pi(kr)^2}, \qquad k = 2\pi/\lambda, \tag{8}$$

and λ is the wavelength. A multispectral inversion technique[22] is applied to this step. From the volume spectrum thus obtained, we can calculate the phase function and the optical thickness of aerosols for the next step and (5) repeat steps (1)–(4) until a convergence criterion is satisfied.

By this algorithm, columnar volume spectrum and related optical characteristics, i.e., optical thickness and phase function, of aerosols above a flight level can be retrieved from spectral intensities in the solar meridional plane as well as in the solar almucantar. Several test calculations adopting the scattering angles of $\theta = 3\,(1)\,10\,(2)\,20\,(5)\,30°$ and twenty-particle radii with equilog-spacing from 0.03 to 30 μm showed that the volume spectrum between radii from 0.2 to 2 μm can be retrieved from aureole intensities measured for the scattering angles $5° \le \theta \le 30°$.[27]

The normalized kernel functions for the differential scattering coefficient, $K(\theta,x)/\int K(\theta,x)dx$, are shown in Fig. 2 together with the normalized kernel function for total extinction, $K_e(\lambda,x)/\int K_e(\lambda,x)dx$, where K_e is the kernel of the integral equation

$$\tau_a = \int K_e(\lambda,x)v(x)dx \tag{9}$$

and related to the Mie's efficiency factor for extinction $Q_e(kr)$ by

$$K_e(\lambda,x) = \frac{3}{4r}Q_e(kr). \tag{10}$$

From the figure we can see that the inversion of the spectral extinction data is approximately equivalent to the inversion of the spectrum of $\beta_a(\theta)$ at a single-scattering angle around 30°. We, therefore, use the

Table II. Flight Log of Airborne Measurements

Date	Location	Alt. (km) Pres. (mb)	Aircraft
JAN 14 1984	Nagoya 35.2°N, 136.7°E	5.18 515	CESSNA 206
FEB 16	Yao 34.5- 29.6°N 135.5-135.0°E	6.04 478	MERLIN IV
AUG 7,8	Yao-Iwo-jima 34.5- 19.9°N 135.5-141.2°E	5.06 557	MERLIN IV
NOV 7,8	Nagoya 35.2°N, 136.7°E	7.07 414	CESSNA 206
SEP 26 1985	Biwako 35.4°N, 136.2°E Wakasa 35.8°N, 135.9°E	6.38 455	CESSNA 206
OCT 9	Nagoya 35.2°N, 136.7°E	6.19 466	CESSNA 206

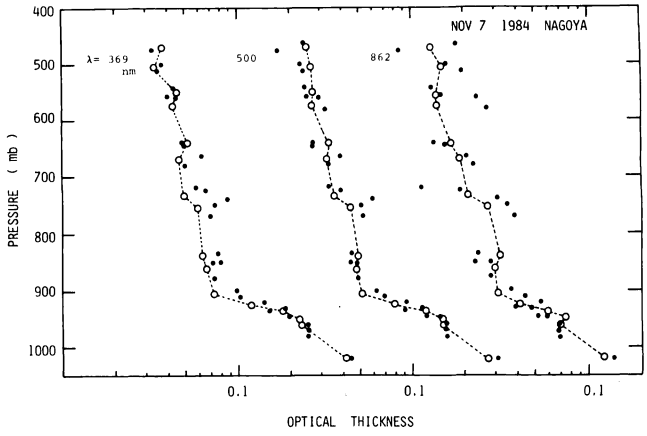

Fig. 3. Vertical profiles of the aerosol optical thickness in the layer between a flight level and the top of the atmosphere. Closed and open circles show values obtained from the direct and diffuse solar radiations, respectively, in the first ascent on 7 Nov. 1984.

multispectral aureole intensities for the inversion instead of adopting erroneous spectral extinction data simultaneously with the aureole data.

III. Results and Discussion

Several aircraft observations were carried out in 1984 and 1985 as shown in Table II using Swerlingen Merlin IV and Cessna 206 aircrafts as part of the aircraft measurement program in the Japanese Middle Atmosphere Program. Vertical flights over Nagoya and horizontal flights along the longitudes of 135 and 140°E were adopted to observe the vertical–horizontal structure of the optical stratification of aerosols over Japan. The aureolemeter was mounted on top of the Merlin IV aircraft and in the rear space of the Cessna 206 aircraft removing the rear glass window. For the flights on 7 and 8 Aug., the scanning along the meridional plane of the sun was adopted because of high solar elevation, while the scanning along the solar almucantar was used for other flights. For these data we have retrieved the columnar volume spectrum, optical thickness, and phase function of aerosols above the flight level.

In Fig. 3, we compare the vertical profile of the aerosol optical thickness obtained by the present method with that obtained from the direct solar radiation. In the latter method (the direct method), the optical thickness is calculated from Eq. (3) with a calibration constant F_0 for each wavelength tuned so as to fit the values of the optical thickness with those estimated from the present method above the haze layer. Values of the optical thickness obtained by the direct method scatter closely around the profiles estimated by the present method, although the error increases with an increase of height and wavelength. Without this tuning, the results of the direct method often become negative or unrealistically large for the calibration constants F_0 determined preliminarily on the ground by a modified long method.[13] This fact shows that the optical thickness obtained by the present method was a good estimate of the optical stratification of aerosols, whereas the optical thickness obtained by the direct method tends to be marred by *in situ* noises of several origins. Close investigation, however, shows some systematic disagreement between the results of both methods. One possible reason for this disagreement may be a horizontal inhomogeneity in the aerosol loading and in the optical properties of aerosols, because the present method assumes a plane–parallel atmosphere exists above the flight level and a Lambertian layer below the flight level. The complex refractive index of aerosols was assumed to be $m = 1.45–0i$, and the albedo of the underlying layer was measured by cooperated spectral pyranometers.[28] Since the imaginary index of refraction is assumed to be zero, the optical thickness for scattering is identical to the optical thickness for extinction shown in Fig. 3.

Figures 4 and 5 show typical examples of the aureole intensity as a function of the scattering angle at $\lambda = 500$ nm and as a function of the wavelength at $\theta = 20°$, respectively. Retrieved values coincide fairly well with the observed value. The rms deviations are 4.9% at most as an average of the five spectral channels from 368 to 862 nm. It is noteworthy that the retrieved optical thickness for scattering was a smooth function of the wavelength reflecting smooth spectral profiles of the aureole intensity shown in Fig. 5, while the optical thickness obtained by the direct method often showed a doubtful irregular spectrum.

In Fig. 6 we summarize the obtained vertical profiles of the optical thickness for scattering at $\lambda = 500$ nm. Error bars show the rms deviation among two to eight data points within adjacent levels of two to four flight legs. For the profile on 14 Jan. 1984 the data points were smoothly connected without error bars because of the scarcity of original data. It is found that the rms deviations were ~10%, and the optical stratifications were steady during each flight for 2–3 h. Comparing profiles of successive days, it is found that the optical stratification did not change rapidly at the level as high as 500 mb, while it changed by a factor as large as 4 during one day in the lower troposphere, suggesting a large vertical difference in the time scale of variation of the optical stratification of aerosols.

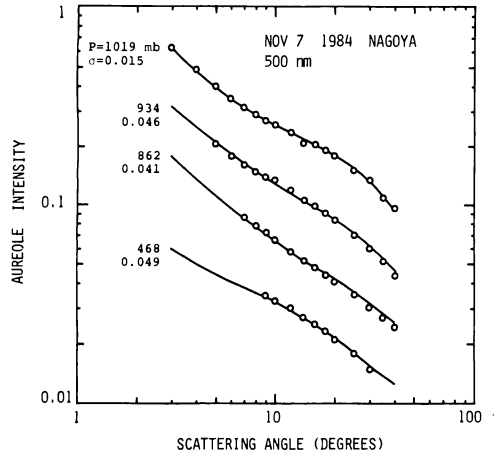

Fig. 4. Observed (circles) and retrieved (solid lines) aureole intensities in the solar almucantar at λ = 500 nm as a function of the scattering angle. Values at pressures of 1019, 934, 862, and 468 mb with the rms deviation σ are displayed. Data: 7 Nov. 1984.

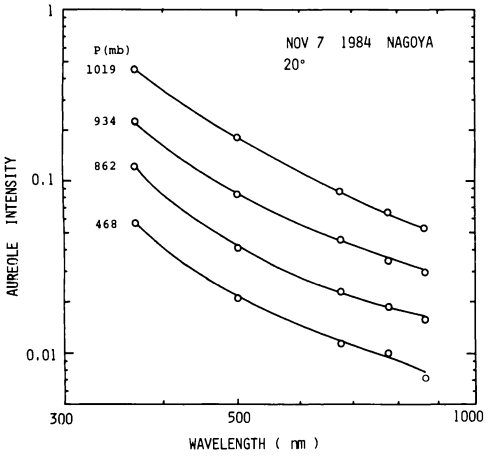

Fig. 5. Same as Fig. 4 but at $\theta = 20°$ and as a function of wavelength.

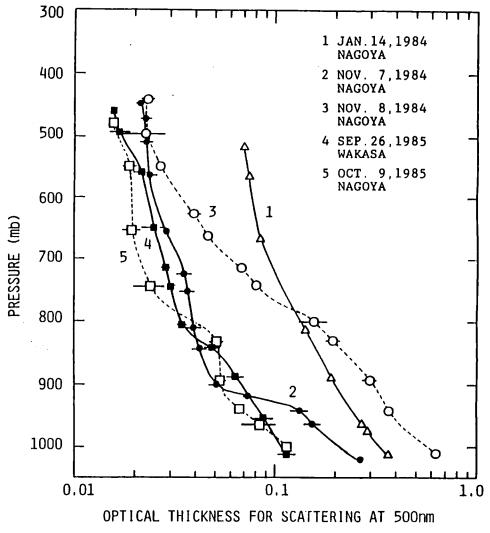

Fig. 6. Vertical profile of the aerosol optical thickness at λ = 500 nm.

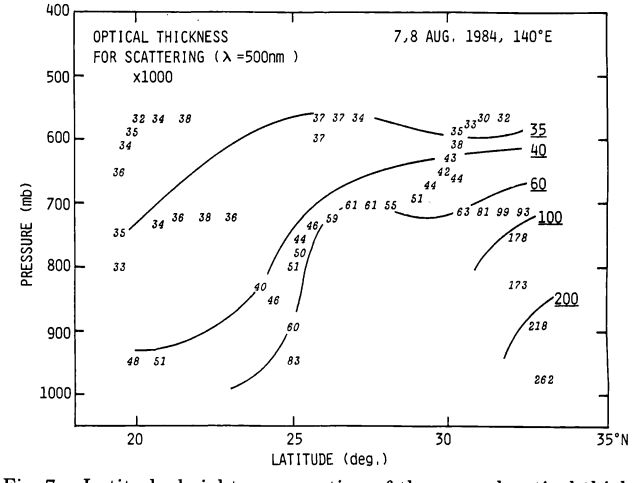

Fig. 7. Latitude–height cross section of the aerosol optical thickness in per mill at λ = 500 nm along 140°E. Data: 7 and 8 Aug. 1984.

Figure 7 shows a latitude–height cross section of the optical depth of aerosols at λ = 500 nm along the longitude of 140 E, obtained by the flights on 7 and 8 Aug. 1984. The effect of aerosols of ground origin was found to be significant at levels lower than 650 mb and northward of 25°N. Observations by a particle counter in the summer season[29] and an aerosol sampler in the winter season[30] showed a similar tendency with somewhat abrupt clearing of the air at locations around 26°N, suggesting a aerosol lifetime of several days.

From Fig. 7, it is recommended that we should utilize isolated islands offshore ~1000 km from the contaminated area or the aircraft with flight levels above 550 mb for monitoring stratospheric aerosols. To see the large scale latitudinal distribution of the optical stratification of background aerosols, we show in Fig. 8 the optical depth of aerosols at levels higher than 550 mb. In the summer season the distribution of aerosols was relatively independent of the latitude, while some latitudinal tendency appeared in the winter season.

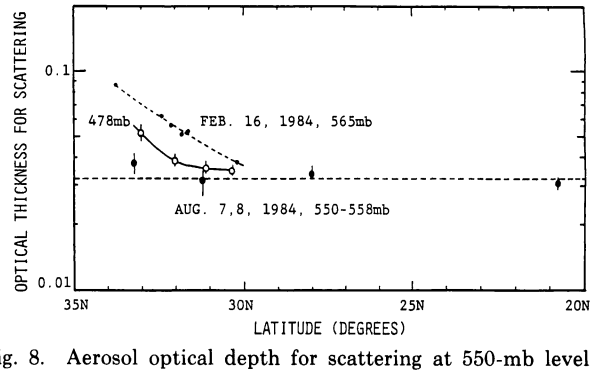

Fig. 8. Aerosol optical depth for scattering at 550-mb level vs latitude. Data: 16 Feb. 1984 (O at 478 mb and • at 565 mb); 7, 8 Aug. 1984 (●).

An expected reason for this tendency may be the difference in the large scale wind system in different seasons. In winter, a strong NW wind blows steadily, and soil derived aerosols originating from the Chinese

continent and Japanese islands are lifted into the free atmosphere. Although not shown in a figure, volume spectra retrieved by our scheme and particle numbers obtained by an optical particle counter suggested that large particles were abundant at an upper troposphere on these days.

Figure 9 shows the time series of the aerosol optical depth for scattering at 550 mb. During two years of observation the optical depth decreased steadily, suggesting that the El Chichon dust cloud was responsible for a large part of the optical depth of 550 mb. The displayed decreasing tendency is similar to other investigations shown in Fig. 9, i.e., optical thicknesses obtained by an aureolemeter at Syowa Station, Antarctica[31] and retrieved from the lidar observation at Tsukuba, Japan.[32] The value of the e-folding time of the optical thickness due to El Chichon aerosols is estimated from Fig. 9 as 280 days for the period from Feb. to Nov. 1984 assuming that the effect of El Chichon aerosols disappeared in Oct. 1985. This value of the e-folding time is consistent with other observations.[33,34]

Figure 10 shows the time series of the retrieved volume spectrum of aerosols at a height of 550 mb with a lognormal function superimposed on the Junge size distribution as

$$v(\ln r) = C \exp\{-[\ln(r/a)/\ln s]^2/2\} + C_J, \qquad (11)$$

where C, a, and s are the coefficient, mode radius, and standard deviation of the lognormal volume spectrum, and C_J is the coefficient of the Junge size distribution which is a constant in terms of the volume spectrum. Integration of Eq. (9) over radii from 0.05 to 30 μm showed that the retrieved optical thicknesses can be interpreted by Eq. (11) with an error of <10% for values of C, a, s, and C_J shown in Fig. 10. The tendency of the time series shows that aerosols of lognormal mode gradually disappeared decreasing its mode radius from 0.58 to 0.35 μm, and the Junge mode prevailed in the fall of 1985. Although the sun-shading hood of the aureolemeter was modified in June 1984, the tendency was not affected by this change, suggesting that contamination of the signal from the reflection in the sun-shading hood is not considered the reason for this tendency. Furthermore, we carefully limited the significant range of the particle radius for display within $0.1 \le r \le 2\,\mu$m, because the hood contamination affects significantly the retrieved volume spectrum of larger particles. A closed investigation of the results of inversion showed that no significant contributions were expected from outside the displayed radius range. Reported values of the mode radius and the standard deviation of El Chichon aerosols are (a,s) = (1.44,2.25) for an 18–21.5-km altitude on 28 Jan. 1983 at Laramie, WY[33] (0.55,1.4) in Jan., Feb. 1983, (0.67,1.3) in Mar. 1983 at Richland, WA,[35] and (0.47,1.3) in Jan. 1983 at Tsukuba, Japan[36] in terms of the lognormal fitting of the volume spectrum. Considering the growth of El Chichon aerosols,[33] our result in Fig. 10 is consistent with these values. If we identify the lognormal mode of the displayed volume spectra in Fig. 10 as El Chichon aerosols, we can calculate the total columnar mass of El Chichon aerosols from Eq. (11) by integrating the lognormal function with the particle radius assuming a density of 1.6 g/cm^3 as shown in Fig. 11. In the figure we also plotted the result obtained by Hofmann and Rosen[33] by particle counters. The value of 0.0074 g/m^2 on 16 Feb. 1984 is consistent with the result of the particle counters, and the value of the e-folding time of the columnar mass is estimated as 230 days, which is the nearly same value for Fig. 9, suggesting that the time series in Fig. 10 obviously reflected

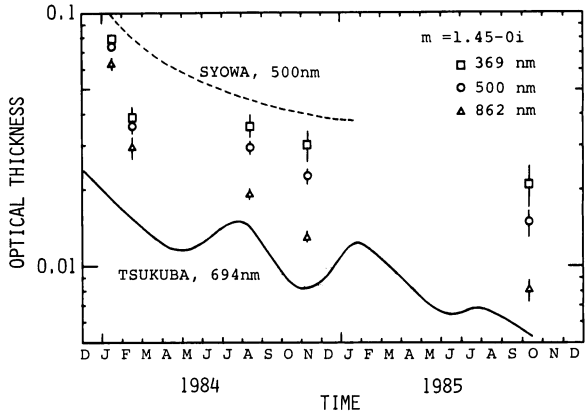

Fig. 9. Time series of the aerosol optical depth at a 550-mb level for λ = 368 (□), 500 (○), and 862 (△) nm. Optical thickness measured at Syowa Station, Antarctica (dashed line) and that retrieved from lidar measurements at Tsukuba, Japan (solid line) are also shown.

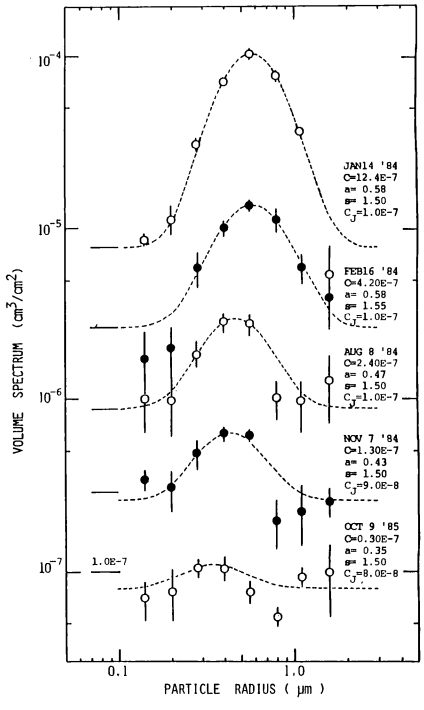

Fig. 10. Time series of the retrieved volume spectrum of aerosols at 550-mb level vs the particle radius in microns. Best fits of the lognormal function defined in Eq. (11) are shown by dotted lines.

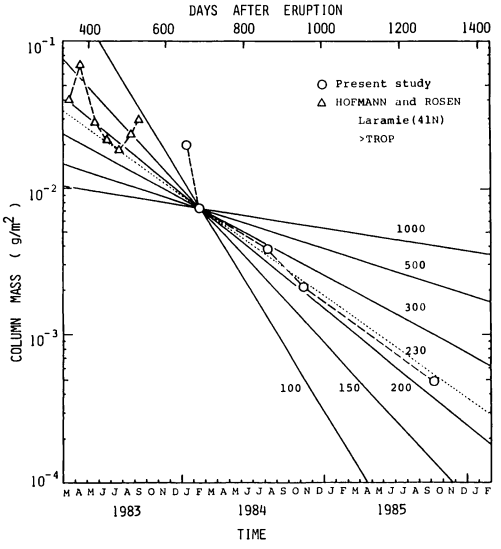

Fig. 11. Aerosol column mass above 550-mb level (O) in the present study and above tropopause (Δ) by Hofmann and Rosen as a function of time (lower scale) or days after the eruption (upper scale). Exponential decaying profiles with several e-folding times from 100 to 1000 days are also shown by straight lines.

the stratospheric El Chichon aerosols. In this context it is noteworthy that the significant variation of the spectrum of the optical thickness shown in Fig. 9 was caused by the competing effects of the two modes, i.e., El Chichon aerosols and the background Junge aerosols, and the effect of the change in the volume spectrum of the El Chichon aerosols was relatively insignificant. It may be concluded from these considerations that the effect of El Chichon aerosols persisted until fall 1985.

IV. Summary

We have shown observed results by an airborne multispectral aureolemeter and discussed some features of the background aerosols in terms of the optical thickness and retrieved volume spectrum. Especially, it has been found that the optical stratification above the 550-mb level was significantly modified by El Chichon aerosols until Oct. 1985. El Chichon aerosols had a lognormal-type volume spectrum and decayed with an e-folding time of ~230–280 days while decreasing their mode radius from 0.58 to 0.35 μm and maintaining a standard deviation of 1.5 during the observation period.

In Table III we summarize results of the analysis for altitudes above 550 mb. As expected from the values of the rms deviations of the optical thickness, our results are of high precision and reflected well the optical stratification of aerosols over Japan during the observation period. The backscattering ratio defined as $\tau_a/\beta_a(180)$ and the first two coefficients x_m of a Legendre expansion of the phase function of aureolemeters,

$$P_a(\theta) = \frac{1}{4\pi}\sum_m (2n+1)x_m p(\cos\theta),$$

Table III. Optical Thickness for Scattering, Backscattering Ratio, and First Two Coefficients of Legendre Expansion of the Phase Function of Aerosols; Parameters of the Power-Law Fitting of the Spectrum of the Optical Thickness and the Lognormal Fitting of the Volume Spectrum are also Shown

DATE	JAN14,84	FEB16,84	AUG 8,84	NOV 7,84	OCT 9,85
PRESSURE	540	478	557	458	478
OPTICAL THICKNESS FOR SCATTERING					
368	0.0791±25	0.0393±34	0.0356±44	0.0298±43	0.0212±41
500	0.0736±22	0.0357±23	0.0294±20	0.0227±14	0.0150±20
675	0.0699±36	0.0330±20	0.0240±10	0.0173± 5	0.0108±13
777	0.0663±37	0.0312±24	0.0213± 8	0.0149± 4	0.0092±10
862	0.0626±37	0.0294±28	0.0192± 6	0.0131± 3	0.0081± 9
BACKSCATTERING RATIO					
368	23.2±0.4	23.2±3.7	27.3±3.6	29.5±4.1	29.9±4.3
500	28.2±0.7	27.3±5.2	31.8±4.0	33.3±5.3	30.9±5.2
675	37.5±0.2	34.2±5.2	37.3±3.6	38.2±6.4	31.8±4.0
777	43.2±0.4	38.1±4.6	39.3±3.8	39.9±6.9	31.7±3.0
862	47.3±0.9	40.6±4.2	40.4±4.3	40.7±7.3	31.7±2.4
1ST MOMENT OF PHASE FUNCTION					
368	0.654±40	0.666±32	0.657±50	0.641±63	0.635±75
500	0.685±21	0.690±18	0.686±27	0.668±38	0.650±53
675	0.714± 8	0.714± 7	0.703± 9	0.686±18	0.664±25
777	0.723± 6	0.721± 7	0.703± 6	0.686±12	0.665±15
862	0.724± 4	0.723±10	0.700± 7	0.683± 9	0.664±10
2ND MOMENT OF PHASE FUNCTION					
368	0.521±42	0.528±32	0.503±45	0.478±63	0.461±73
500	0.545±17	0.547±16	0.527±17	0.502±31	0.482±40
675	0.557± 6	0.557± 9	0.529± 4	0.506± 7	0.490±14
777	0.553± 4	0.554±14	0.520± 6	0.496± 2	0.485±10
862	0.546± 4	0.548±18	0.509± 7	0.486± 5	0.481±10
POWER LAW FITTING					
α	0.26	0.33	0.71	0.95	1.13
s_{500}	0.0737	0.0358	0.0290	0.0225	0.0150
LOG-NORMAL VOLUME SPECTRUM					
C	1.24E-6	4.20E-7	2.40E-7	1.30E-7	0.30E-7
a	0.58	0.58	0.47	0.43	0.35
s	1.50	1.55	1.50	1.50	1.50
C_J	1.00E-7	1.00E-7	1.00E-7	0.90E-7	0.80E-7

are also calculated from the retrieved volume spectra. In Table III we also show fitting parameters of the spectrum of the optical thickness by the form $\omega_{0a}\tau_a = s_{500}(500/\lambda)^\alpha$ and fitting parameters in Eq. (11). As is well known, the parameter α is related to the exponent of the effective power-law size distribution as $3 + \alpha$. The time variation of the parameters s_{500} and α shows that the stratospheric sky was turbid and whitened in the winter of 1984, and the normal blue sky prevailed in the fall of 1985.

From discussions in the preceding sections, our airborne aureolemeter was found to be a useful instrument for monitoring the large scale optical stratification of aerosols, although the volume spectrum of larger particles cannot be retrieved due to the lack of information from small scattering angles. We are now developing a revised version of the aureolemeter, which has a smaller minimum observable angle. Using these instruments in cooperation with the lidar and satellite systems, a more comprehensive analysis should be made in the future to make clear some speculations presented in this study.

I. Tabata and M. Shiobara of the Meteorological Research Institute are gratefully acknowledged for providing their original data of the optical thickness and for valuable discussions. Personnel and the flight facility of Syowa Aviation Co. and Nakanihon Aviation Co. are acknowledged for their efforts during the mounting and experimental period.

This research was supported by Funds for the Middle Atmosphere Program (MAP) from the Ministry of Education, Science and Culture, Japan.

References

1. M. I. Budyko, "The Effect of Solar Radiation Variation on the Climate of the Earth," Tellus **21,** 611 (1969).
2. J. B. Pollack, O. B. Toon, C. Sagan, A. Summers, B. Baldwin, and W. V. Camp, "Volcanic Explosions and Climatic Change: A Theoretical Assessment," J. Geophys. Res. **81,** 1071 (1976).
3. J. Hansen, D. Johnson, A. Lacis, S. Lebedeff, P. Lee, D. Rind, and G. Russell, "Climatic Impact of Increasing Atmospheric Carbon Dioxide," Science **213,** 957 (1981).
4. R. P. Turco, R. C. Whitten, and O. B. Toon, "Stratospheric Aerosols: Observation and Theory," Rev. Geophys. Space Phys. **20,** 233 (1982).
5. J. D. Spinhirne, "El Chichon Eruption Cloud: Latitudinal Variation of the Spectral Optical Thickness for October 1982," Geophys. Res. Lett. **10,** 881 (1983).
6. E. Dutton and J. DeLuisi, "Spectral Extinction of Direct Solar Radiation by the El Chichon Cloud during December 1982," Geophys. Res. Lett. **10,** 1013 (1983).
7. G. M. Shah and W. F. J. Evans, "Latitude Survey of Aerosol Optical Thickness of the El Chichon Eruption Cloud in May 1983," Geophys. Res. Lett. **12,** 255 (1985).
8. T. J. Swissler, M. P. McCormick, and J. D. Spinhirne, "El Chichon Eruption Cloud: Comparison of Lidar and Optical Thickness Measurements for October 1982," Geophys. Res. Lett. **10,** 885 (1983).
9. G. Yamamoto and M. Tanaka, "Determination of Aerosol Size Distribution from Spectral Attenuation Measurements," Appl. Opt. **8,** 447 (1969).
10. M. D. King, Harshvardhan, and A. Arking, "A Model of the Radiative Properties of the El Chichon Stratospheric Aerosol Layer," J. Climate Appl. Meteorol. **23,** 1121 (1984).
11. G. E. Shaw, "Error Analysis of Multi-Wavelength Sunphotometry," Pure Appl. Geophys. **114,** 1 (1976).
12. G. E. Shaw, "Sunphotometry," Bull. Am. Meteorol. Soc. **64,** 4 (1983).
13. M. Tanaka, T. Nakajima, and M. Shiobara, "Calibration of Sunphotometer by Simultaneous Measurements of Direct-Solar and Circumsolar Radiations," Appl. Opt. **25,** 1170 (1986).
14. A. Angstrom, "Circumsolar Sky Radiation and Turbidity of the Atmosphere," Appl. Opt. **13,** 474 (1974).
15. M. A. Box, M. H. Reich, S.-Y. Lo, and B. H. J. McKellar, "Atmospheric Turbidity and the Circumsolar Radiation," Appl. Opt. **16,** 341 (1977).
16. N. T. O'Neill and J. R. Miller, "Combined Solar Aureole and Solar Beam Extinction Measurements. 1: Calibration Considerations," Appl. Opt. **23,** 3691 (1984).
17. J. I. Gordon, "New Uses for the Solar Almucanter," Appl. Opt. **24,** 3381 (1985).
18. J. T. Twitty, "The Inversion of Aureole Measurements to Derive Aerosol Size Distributions," J. Atmos. Sci. **32,** 584 (1975).
19. G. E. Shaw, "Inversion of Optical Scattering and Spectral Extinction Measurements to Recover Aerosol Size Spectra," Appl. Opt. **18,** 988 (1979).
20. G. E. Shaw, "Optical Chemical and Physical Properties of Aerosols over the Antarctic Ice Sheet," Atmos. Environ. **14,** 911 (1980).
21. A. Deepak, M. A. Box, and G. P. Box, "Experimental Validation of the Solar Aureole Technique for Determining Aerosol Size Distributions," Appl. Opt. **21,** 2236 (1982).
22. T. Nakajima, M. Tanaka, and T. Yamauchi, "Retrieval of the Optical Properties of Aerosols from Aureole and Extinction Data," Appl. Opt. **22,** 2951 (1983).
23. N. T. O'Neill and J. R. Miller, "Combined Solar Aureole and Solar Beam Extinction Measurements. 2: Studies of the Inferred Aerosol Size Distributions," Appl. Opt. **23,** 3697 (1984).
24. J. T. Twitty, R. J. Parent, J. A. Weinman, and E. W. Eloranta, "Aerosol Size Distributions: Remote Determination from Airborne Measurements of the Solar Aureole," Appl. Opt. **15,** 980 (1976).
25. J. J. DeLuisi *et al.*, "Results of a Comprehensive Atmospheric Aerosol-Radiation Experiment in the Southwestern United States. Part I: Size Distribution, Extinction Optical Depth and Vertical Profiles of Aerosols Suspended in the Atmosphere," J. Appl. Meteorol. **15,** 441 (1976).
26. T. Nakajima and M. Tanaka, "Matrix Formulations for the Transfer of Solar Radiation in a Plane-Parallel Scattering Atmosphere," J. Quant. Spectrosc. Radiat. Transfer **35,** 13 (1986).
27. T. Nakajima, M. Tanaka, and T. Hayasaka, "Retrieval of the Optical Thickness and the Volume Spectrum from the Solar Aureole Intensity," (in preparation).
28. M. Tanaka, T. Hayasaka, and T. Nakajima, "Estimation of the Imaginary Index of Refraction from the Airborne Pyranometer Measurements," (in preparation).
29. T. Takamura and M. Miyazaki, "Measurements of the Vertical and Horizontal Profiles of Aerosols over the Pacific Ocean near Japan Island," Tech. Rep. Sci. Tech. Natl. Defence Acad. **19,** 1 (1981).
30. T. Ohkita, Ed., "Residence Time of Aerosols," Report of Research Project, Grant in Aid for Scientific Research B158-R11-1 (1983), p. 98.
31. M. Shiobara, Meteorological Research Institute, Tsukuba, Japan, private communication.
32. I. Tabata, Meteorological Research Institute, Tsukuba, Japan, private communication.
33. D. J. Hofmann and J. M. Rosen, "On the Temporal Variation of Stratospheric Aerosol Size and Mass During the First 18 Months Following the 1982 Eruption of El Chichon," J. Geophys. Res. **89,** 4883 (1984).
34. S. Hayashida and Y. Iwasaka, "On the Long Term Variation of Stratospheric Aerosol Content After the Eruption of Volcano El Chichon: Lidar Measurements at Nagoya, Japan," J. Meteorol. Soc. Jpn. **63,** 465 (1985).
35. J. J. Michalsky, B. M. Herman, and N. R. Larson, "Mid-Latitude Stratospheric Aerosol Layer Enhancement by El Chichon: The First Year," Geophys. Res. Lett. **11,** 76 (1984).
36. S. Asano, M. Sekine, M. Kobayashi, and K. Murai, "Atmospheric Turbidity and Aerosol Size Distribution in Winter at Tsukuba: Effects of the Eruption of El Chichon," J. Meteorol. Soc. Jpn. **63,** 453 (1985).